UNSTRUCTURED MESH SOLVERS FOR HYPERBOLIC PDES WITH SOURCE TERMS: ERROR ESTIMATES AND MESH QUALITY

M. BERZINS
School of Computer Studies,
University of Leeds,
Leeds LS2 9JT, U.K.
Email: martin@scs.leeds.ac.uk

AND

L.J.K. DURBECK
Department of Computer Science,
University of Utah, USA.
Email: ldurbeck@cs.utah.edu

Abstract. The solution of hyperbolic systems with stiff source terms is of great importance in areas such as atmospheric dispersion. The finite-volume approach used here for such problems employs Godunov-type methods, a sophisticated splitting approach for efficiency and adaptive tetrahedral meshes to provide the necessary resolution for physically meaningful solutions. This raises the issues of how to estimate the error for Godunov type methods and what is an appropriate mesh for such applications. A new mesh visualization and haptic-interface tool will be shown to help clarify this and its use illustrated for a model problem in three space dimensions.

1. Introduction

Unstructured triangular and tetrahedral meshes are widely used in engineering and scientific computing for solving problems via finite element and finite volume methods. At the same time Godunov methods are widely used in the solution of problems with hyperbolic parts (Godlewski and Raviart, 1996; Kröner, 1997; Toro, 1999). The intention here is to consider some of the issues that arise from combining these approaches when solving problems such as the 3D advection reaction problem, taken from a model of atmospheric dispersion from a power station plume - a concentrated source of NOx emissions, (Tomlin, 1999). The photo-chemical reaction of this NOx with polluted air leads to the generation of ozone at large distances downwind from the source. An accurate description of the distribution of pollutant concentrations is needed over large spatial regions in order to compare with field measurement calculations. The complex chemical kinetics in the atmospheric model gives rise to sudden changes in the concentration of the chemical species in both space and time. These changes must be matched by changes in the spatial mesh and the timesteps if high resolution is required, (Tomlin, 1999). The effects of the plume interestingly causes levels of ozone to rise above the background levels at quite large distances downwind from the source of NOx. This application is modelled by the atmospheric diffusion equation in three space dimensions given by:

$$\frac{\partial c_s}{\partial t} + \frac{\partial u c_s}{\partial x} + \frac{\partial v c_s}{\partial y} + \frac{\partial w c_s}{\partial z} = D + R_s + E_s - \kappa_s c_s, \tag{1}$$

where c_s is the concentration of the s'th compound, u,v and w, are wind velocities and κ_s is the sum of the wet and dry deposition velocities. E_s describes the distribution of emission sources for the s'th compound and R_s is the chemical reaction term which may contain nonlinear terms in c_s. D is the diffusion term. For n chemical species a set of n coupled partial differential equations (p.d.e's) is formed.

The solution techniques employed consist of time integration methods specially designed for explicit convection and implicit source terms handled by using a very efficient Gauss-Seidel iteration. Finite volume cell-vertex and cell-centred Godunov-type schemes (Godunov, 1959; Van Leer, 1984) are both used for space discretization. For this atmospheric diffusion model, the meshes and means of obtaining them are described in (Johnson, 1998; Speares, 1997). The advantage of the Godunov-type methods based on upwinding and approximate Riemann problems is that it is possible to preserve positivity of the solution - a key requirement for reacting flow problems. Mesh adaptation using h refinement, even based on simple gradient information gives dramatically improved solutions, see (Tomlin, 1999) but raises the issue of whether or not the mesh is appropriate for all the species.

The only sure way of knowing whether or not the mesh is appropriate is to use error indicators and to understand how the error depends on both the solution and on element shape, preferably by visualization. It is hard to visualize all the mesh elements in a full 3D mesh display and it is difficult to comprehend fully the myriad of element shapes and sizes, see Figure 1. The combined haptic and visual interface of (Durbeck, 1999) has been designed to overcome the daunting task of finding "bad" tetrahedra in a visually complex mesh. In the remainder of this paper an error indication approach will be outlined and used in combination with the visual interface to find bad tetrahedra in a 3D adaptive unstructured mesh.

2. Adaptive Numerical Solution Techniques.

In order to illustrate the approaches consider the simple 3D advection equation

$$U_t + aU_x + bU_y + cU_z = 0 \tag{2}$$

The numerical method employed is a first order accurate, conservative cell-centred finite volume scheme. The numerical solution in element i at time t_n is denoted by u_i^n, and is an approximation to the exact element averaged volume integral of the solution, (Speares, 1997), over V_i the volume of element i, and is usually regarded as being valued at the element centroid for cell centred schemes. The numerical solution at the next time level t^{n+1} may be written as:

$$u_i^{n+1} = u_i^n - \delta t F_i(t_n, \underline{u}) \quad \text{where} \quad \mathrm{F_i(t_n, \underline{U})} = \frac{1}{\mathrm{V_i}}, \sum_{\mathrm{k}=0}^{3} \mathrm{A_k}\mathbf{F}_\mathrm{k}.\mathbf{n}_\mathrm{k} \tag{3}$$

and where the sum is over the k faces of the element i. The $\mathbf{n}_k$ are the outward face unit normal vectors and A_k the face areas. The fluxes $\mathbf{F}_k$ represent the numerical flux function for each element face, termed the element face fluxes, and are determined by the scheme. In the case of the Godunov scheme these element face numerical fluxes are constructed from the solution of the local element Riemann Problem (RP) at each element face, see (Godunov, 1959; Speares, 1997). In the calculations described here both first and second order schemes are used, (Van Leer, 1984).

A standard method for choosing the timestep in the numerical solution of p.d.e.s is to use a CFL condition. Although such a condition may ensure stability it may be imprecise as an accuracy control, particularly when complex chemistry source terms are present in the p.d.e. problem. It is important to use an error control which reflects the spatial and temporal contributions to the error incurred.

The global error in the numerical solution can be expressed as the sum of the spatial discretization error, and the global time error, Efficient time integration requires that the spatial and temporal are roughly the same order of magnitude. The need for spatial error estimates to be unpolluted by temporal error requires the spatial error to be the larger of the two errors. One approach for achieving this is described by, (Berzins, 1995), who balances the spatial and temporal errors by controlling the local time error to be a fraction of the local growth in the spatial discretization error.

The local-in-time spatial error, $\underline{\hat{e}}(t_{n+1})$, for the timestep from t_n to t_{n+1} is defined as the spatial error at time t_{n+1} given the assumption that the spatial error, $\underline{e}(t_n)$, is zero. The error $\underline{\hat{e}}(t_{n+1})$ is estimated by the difference between the computed solution and the first-order solution which satisfies an o.d.e. system given by

$$\dot{\underline{v}}_{n+1}\ (t) = \underline{F}_N^*(t, \underline{v}_{n+1}(t)), \tag{4}$$

where $\underline{v}_{n+1}(t_n) = \underline{V}(t_n)$ and where $\underline{F}_N^*(.,.)$ is obtained by using the limiter function $\Phi(.)$ in the spatial discretization method, (zero for a first order scheme), to be that for a second order scheme. The local-in-time space error is estimated by

$$\underline{\hat{e}}(t_{n+1}) = \underline{V}(t_{n+1}) - \underline{v}_{n+1}(t_{n+1}) \tag{5}$$

and is computed by applying, say, the forward Euler method method to equation (4), thus giving (with one evaluation of $\underline{F}_N^*(.,.)$ per timestep):

$$\underline{\hat{e}}(t_{n+1}) = \delta t[\underline{F}_N(t_n, \underline{V}(t_n)) - \underline{F}_N^*(t_n, \underline{V}(t_n))]. \tag{6}$$

While reliable error estimators for finite volume unstructured mesh solvers exist for simple problems, e.g. (Kroner, 2000), there are no such estimators for problems with complex source terms. Consequently, we are forced to rely instead on local error indicators such as those described above. For problems without source terms the estimate of Kroner and Ohlberger may be adapted to estimate this local in time space error. Let $\hat{e}(t)$ be the local in time spatial error computed on a timestep then combining the estimates of Corollary(2.14) of (Kroner, 2000) and the ideas of (Berzins, 1995) gives

$$\int\int\int_V \hat{e}(t_{n+1}) d\tau = a\ \delta t\ h^2\ Q + 2\sqrt{b\ c\ \delta t\ h^2\ Q} \tag{7}$$

where a, b, c are constants, see (Kroner, 2000) and for an evenly spaced mesh with spacing h and timestep δt the value of Q is given by

$$Q = \sum_{j \epsilon NT} h|u_j^{n+1} - u_j^n| + L \sum_{E \epsilon NT} (\delta t + h)|u_j^n - u_l^n|$$

where L is a constant, u_j^n is the solution value associated with the jth tetrahedron out of a mesh of NT tetrahedra with edges $E \epsilon NT$ at time t_n. The important feature of this error estimator is that, apart from the constants, the only solution information used consists of solution jumps across faces i.e. $u_j^n - u_l^n$ and solution changes in time $u_j^{n+1} - u_j^n$ on a particular tetrahedron. However the estimate does not reflect the fact that

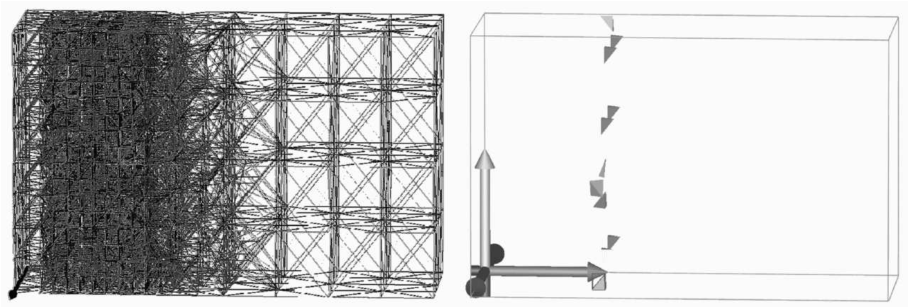

Figure 1. (a) Wire frame mesh and (b) visualization of poor elements

face orientation in flow problems is critical as error may not be convected through faces aligned with the flow.

2.1. A SIMPLE 1D ADVECTION EQUATION EXAMPLE

Consider the advection of a simple one-dimensional discontinuity moving from left to right in a 3D channel, as defined by equation (2) with $a = 1, b = c = 0$. A typical example of a 3D unstructured mesh with 16,000 elements. is shown in Figure 1a. The mesh is shown in wire frame, with all the nodes and their attachments shown, and has been refined about the disconitinuity.

It is of interest to evaluate the error estimation approaches on a similar simple 1D version of Problem 4 (linear advection) in (Berzins, 1995). The local in time error being measured about halfway across the domain. Figure 2 shows the spatial distribution of the error $\hat{e}(t)$ with the solid line being the true error and the values * showing the error estimate defined by equation (6) and the values + showing the time local error. The peaks in the error graph occur where the scheme smooths the top and bottom of the discontinuity. The figure shows that the error estimator does a good job of estimating the structure and the magnitude of the local-in-time spatial error, particularly as the cfl number is reduced, (Berzins, 1995). of array Table 1 shows the values of the error indicators for different values of the CFL number. The results show that both error estimators do a good job of estimating the L1 norm of the error growth over a single timestep.

3. Visual Mesh Quality Analysis

Error indicators for the simple advection equation example were investigated visually with a user interface developed by (Durbeck, 1999). Durbeck's interface both serves as a visual debugger for the advection mesh and

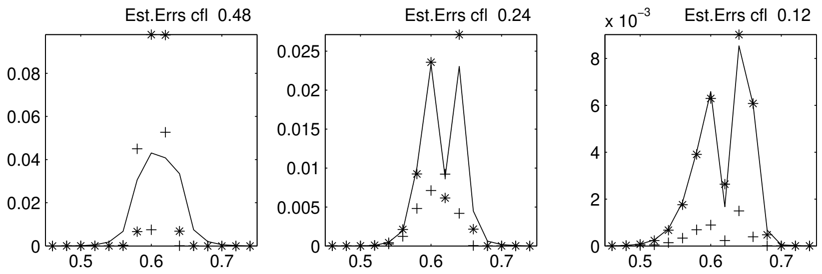

Figure 2. Graphs of local space and time errors

TABLE 1. Comparison of L1 error norm for error indicators

CFL Number	0.96	0.48	0.24	0.12	0.06	0.03
True $\hat{e}$	1.17e-2	3.35e-2	1.46e-3	6.12e-4	2.81e-4	1.33e-4
Berzins eqn(6)	4.53e-2	4.18e-2	1.42e-3	6.23e-4	2.73e-4	1.26e-4
Kroner eqn(7)	1.15e-1	8.13e-2	2.55e-3	8.42e-4	2.85e-4	9.90e-5

presents analytic information about the mesh geometry and error indicators so that the user can deduce the potential causes for poor quality elements. A view of the mesh, reduced via the debugger to its poorest elements, is shown in Figure 1b. The elements are displayed as solids, with lighting and shading effects. The color assigned to each tetrahedron corresponds with its relative error indicator value. Comparison of Figure 1a with 1b indicates that the the poorest elements are roughly aligned and occur near the leading edge of the area refined to represent the discontinuity.

The visual debugger also provides closeups used for analysis of a specific error indicator. The worst element depicted in Figure 1b is shown in closeup view in Figure 3, along with all neighbouring elements which may contribute to its error value. The information presented in this view is intended to correspond closely with the error indicator: in our case, an element's poor quality can be a combination of its shape, orientation and precise vertex locations within the mesh. The same inquiry continues outward to its neighbours and, to a lesser extent, the next level outward as well, as they contribute to the element in question. The worst element and its direct neighbours are displayed as shaded solids and the (less important) next level outward in wire frame. Graphical representations of each element are annotated with the element number, error indicator value, and solution value. Color also provides relative error indicator values. As shown in Figure 3b and 3c, the closeup can be rotated about, and exploded outward from, the central element in order to better view all the tetrahedra.

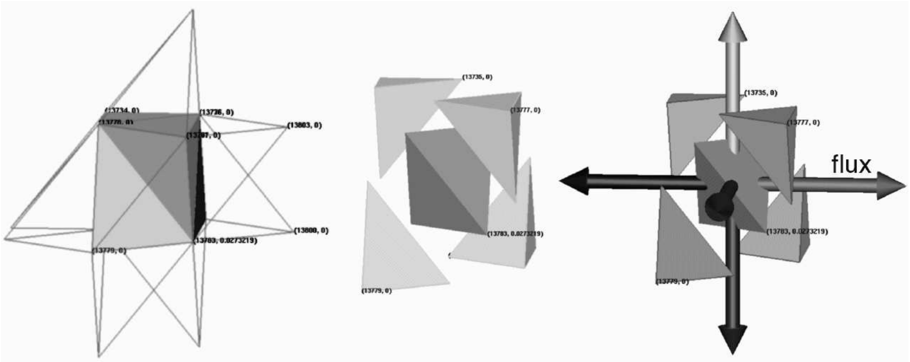

Figure 3. (a) In place (b) exploded (c) rotated closeup views of worst element and its neighbours

As seen in Figure 3, The two main contributors to the central element's high error value appear to be its orientation, which causes two faces to be close to perpendicular to the flux, and the wedge shape of the element, which causes these two faces to be relatively wide. Thus the user has been able to easily identify the cause of poor mesh quality in a complex three dimensional meshes of the type described in Section 1.

References

Berzins M (1995) Temporal Error Control in the Method of Lines for Convection Dominated Equations. *SIAM J. on Sci. Comput.* **16**, pp.558-580.

Durbeck L J K (1999) Contrast Displays: A Haptic and Visual Interface Designed Specifically for Mesh Quality Analysis. M.Sc. Thesis Univ. of Utah.

Godunov S K (1959). A Finite Difference Method for the Computation of Discontinuous Solutions of the Equations of Fluid Dynamics. *Mat. Sb.* **47**, pp 357-393.

Godlewski E and Raviart P A (1996). Numerical Approximation of Hyperbolic Systems of Conservation Laws. Springer.

Johnson C R, Berzins M, Zhukov L, and Coffey R (1998) SCIRun: Applications to Atmospheric Diffusion Using Unstructured Meshes. Numerical Methods for Fluid Dynamics VI. Editor M. J. Baines. ICFD, Oxford Univ. pp111-122.

Kröner D (1997). Numerical Schemes for Conservation Laws. Wiley Teubner.

Kroner D and Ohlberger M (2000) A posteriori error estimates for upwind finite volume schemes for nonlinear conservation laws in multi-dimensions." *Mathematics of Computation*, **69**, pp25-39.

Speares W and Berzins M (1997) A 3D Unstructured Mesh Adaptation Algorithm for Time-Dependent Shock-dominated Problems. *International Journal for Numerical Methods in Fluids* **25** pp81-104.

Tomlin A S, Ghorai S, Hart G and Berzins M (1999) 3-D Adaptive Unstructured Meshes for Air Pollution Modelling. *Environmental Management and Health* 10/4 267-274.

Toro E F (1999). Riemann Solvers and Numerical Methods for Fluid Dynamics. Second Edition, Springer-Verlag.

van Leer B (1984). On the Relation Between the Upwind-Differencing Schemes of Godunov, Enguist-Osher and Roe. *SIAM J. Sci. Stat. Comput.* **5**, pp 1-20.